Comprehensive Model for Randomly Phase-Matched Frequency Conversion in Zinc-Blende Polycrystals and Experimental Results for ZnSe

Taiki Kawamori,[*] Qitian Ru, and Konstantin L. Vodopyanov
CREOL, College of Optics and Photonics, University of Central Florida, Orlando, Florida 32816, USA

Second-order nonlinear interactions in disordered materials based on random phase matching suggest intriguing opportunities for extremely broadband frequency conversion. Here, we present a quantitative realistic model for random phase matching in zinc-blende polycrystals (ZnSe, ZnS, GaAs, GaP, etc.) that takes into account effects of random crystal orientation and grain-size fluctuations, and includes polarization analysis of the generated output. Our simulations are based on rigorous transformation of the second-order susceptibility tensor in randomly rotated coordinates—to account for random orientation of crystalline domains, and demonstrate a good agreement with our experimental data for ZnSe using a nanosecond $\lambda = 4.7$ μm source—in terms of variations of the strength and polarizations of the output fields. Also, it is revealed that random phase matching is most suitable for ultrafast (sub-100-fs) interactions with focused beams, e.g., second-harmonic generation, sum- and difference-frequency generation, and optical parametric oscillation, that typically require short (< 1 mm) interaction lengths, where disordered polycrystals can be on a par, in terms of conversion yield, with ideal quasi-phase-matched crystals.

I. INTRODUCTION

Phase matching is a critical factor for generating new optical frequencies in the coherent process of nonlinear optical frequency conversion [1]. Birefringent crystals have been widely used to compensate phase mismatch, while quasi-phase-matching (QPM) is another technique to maintain the growth of a new optical field by preventing destructive interference. An alternative approach is random phase matching (RPM), which avoids destructive interference by exploiting the random nature of disordered crystalline domains. A wide variety of materials can show this feature as long as they are composed of disordered microstructures that possess second-order nonlinear optical susceptibility. In the early stages of laser development, this was used in a powder technique for the evaluation of nonlinear optical materials [2]. The first frequency conversion in a polycrystalline semiconductor where monocrystals are embedded with random orientations was demonstrated in 1966 and the variation of an output signal in terms of intensity and polarization has been qualitatively discussed [3]. Due to the fact that disordered polycrystalline materials have an extremely wide acceptance bandwidth, they have been used as a nonlinear gain medium for a number of applications, such as nonlinear optical microscopy, autocorrelation measurements,

sum- and difference-frequency generation, and cascade harmonic generation [4–8].

In the field of ultrafast interactions, full advantage has been taken of the ultrawide acceptance bandwidth associated with RPM: a spectrally broad high-average-power (0.3 W) second-harmonic generation (SHG), and also a number of other wave-mixing processes have been observed inside the gain media of mode-locked lasers based on Cr^{2+}-doped polycrystalline zinc sulfide (ZnS) and zinc selenide (ZnSe) samples [9,10]. Most recently, an optical parametric oscillator (OPO) based on RPM has been demonstrated in a ZnSe ceramic, pumped by femtosecond 2.35-μm laser pulses. The OPO produced an ultrabroad spectrum spanning $3 - 7.5$ μm and exhibited a pump depletion as high as 79% [11]. Also, a multioctave spectrum via simultaneous randomly phase-matched three-wave mixing processes, facilitated by filamentation, has been observed in polycrystalline ZnSe [12]. RPM can be viewed as an analogy of a random walk, where the electric field of the output wave grows as the square root of the interaction length within a nonlinear material. Mathematically, the main features of RPM in nonbirefringent polycrystals with randomly oriented domains are the same as in the powder technique first outlined by Kurtz and Perry [2]: namely, (1) the nonlinear conversion yield (in intensity) grows linearly with the sample thickness, (2) the highest conversion is achieved when the average grain size is close to the coherence length L_c, and

---

[*]taikikawamori@knights.ucf.edu

(3) at a fixed sample length and in optimized conditions, the conversion efficiency is higher for greater coherence lengths. Although there have been several attempts to analytically describe the frequency conversion process based on RPM [7,8,13,14], none of them have rigorously derived the probability distribution of the effective susceptibility of a randomly rotated crystal; also, polarization analysis in RPM has been dismissed in these works. In this Letter, we present a model for ultrafast nonlinear $\chi^{(2)}$ interactions in an RPM material that includes random grain orientation and a realistic grain-size distribution, as well as variation of the two orthogonally polarized outputs due to the randomly transformed susceptibility tensor. We also calculate the efficiency of the RPM process normalized to that of an ideal QPM process.

II. RANDOM SECOND-ORDER NONLINEAR SUSCEPTIBILITY

Three-wave mixing in $\chi^{(2)}$ media is characterized by nonlinear polarization, which is expressed as $P_i^{(2)}(\omega) = \epsilon_0 \sum_{jk} \chi_{ijk}^{(2)}(\omega; \omega_1, \omega_2) E_j(\omega_1) E_k(\omega_2)$, where the indexes refer to the principal axes in a crystal coordinate system and $\chi_{ijk}^{(2)}$ is a second-order nonlinear optical susceptibility, which is a third-rank tensor. For zinc-blende semiconductors with a symmetry $\bar{4}3m$, it has six nonzero components for $i \neq j \neq k$, the values of which are all the same under Kleinman symmetry. Because three-wave mixing

processes are reversible and are coupled through the same susceptibility tensor, the RPM analysis for the SHG efficiency is valid for its inverse process—subharmonic OPO [15]. Thus, we use the SHG process for both simulation and experiment, and the results are discussed later for subharmonic femtosecond OPO generation.

The susceptibility variation in each successive grain is modeled by randomly rotated crystal coordinates (x, y, z) with respect to the laboratory frame (x', y', z'). Here, we describe it in three steps, as shown in Fig. 1(a), after setting a random point $(x_0, y_0, z_0) = (\sin\theta\cos\phi, \sin\theta\sin\phi, \cos\theta)$ on a unit sphere in the laboratory frame, such that the probability density per unit surface area is uniform (see below). (1) Start with the crystal's coordinate system, which coincides with that of the laboratory frame. Rotate the crystal coordinate system through angle ϕ around the z axis [Fig. 1(a)]. (2) Rotate the crystal coordinate system through angle θ around its new y axis, so that the new z axis is directed to the point (x_0, y_0, z_0). (3) Rotate the crystal coordinate system through random angle ψ (uniformly distributed between 0 and 2π) around the new z axis. These operations are expressed in Eq. (1) as a product of three successive rotation matrices $R_{\vec{n_1}}(\phi)$, $R_{\vec{n_2}}(\theta)$, and $R_{\vec{n_3}}(\psi)$. Each matrix corresponds to a rotation through an angle ϕ, θ, or ψ (Euler angles) about a fixed axis specified, respectively, by a unit vector defined as $\vec{n_1} = (0, 0, 1)$, $\vec{n_2} = (-\sin\phi, \cos\phi, 0)$, and $\vec{n_3} = (x_0, y_0, z_0)$:

$$R = R_{\vec{n_3}}(\psi)R_{\vec{n_2}}(\theta)R_{\vec{n_1}}(\phi) = \begin{pmatrix} \cos\phi\cos\theta\cos\psi - \sin\phi\sin\psi & -\cos\phi\cos\theta\sin\psi - \cos\psi\sin\phi & \cos\phi\sin\theta \\ \cos\theta\cos\psi\sin\phi + \cos\phi\sin\psi & -\cos\theta\sin\phi\sin\psi + \cos\phi\cos\psi & \sin\phi\sin\theta \\ -\cos\psi\sin\theta & \sin\theta\sin\psi & \cos\theta \end{pmatrix}.$$

(1)

The nonlinear polarization in the laboratory frame is computed by the transformation rule for third-rank tensors, $\chi_{i'j'k'}^{(2)} = R_{i'i}^T R_{j'j}^T R_{k'k}^T \chi_{ijk}^{(2)}$ [16]. In the contracted form, assuming that the fundamental electric field is linearly polarized (parallel to z') and propagates along y', the second-order polarization components that are parallel (along z') and perpendicular (along x') to the input polarization are given by the following:

$$\begin{pmatrix} P_\parallel^{(2)'}(2\omega) \\ P_\perp^{(2)'}(2\omega) \end{pmatrix} = \epsilon_0 E^2(\omega) d_{14} \begin{pmatrix} 6R_{11}R_{21}R_{31} \\ 2R_{11}R_{21}R_{32} \\ +2R_{11}R_{22}R_{31} \\ +2R_{12}R_{21}R_{31} \end{pmatrix}. \quad (2)$$

We perform a Monte Carlo simulation of 1 million iterations for the nonlinear coefficient in a randomly oriented single crystal under the probability conditions $\phi \in [0, 2\pi)$, $\theta = \arccos(u)$, and $\psi \in [0, 2\pi)$ for the Euler angles, where $u \in [-1, 1]$ [17]. These conditions ensure that the probability is uniformly distributed among all possible domain orientations in space. Figure 1(b) shows the distribution of the nonlinear coefficient for both parallel and perpendicular output polarizations in one-dimensional (1D) and two-dimensional (2D) color-coded form with respect to the linearly polarized incoming electric field. The nonlinear coefficient fluctuates within the expected range: $|d_\parallel/d_{14}| \leq \sqrt{4/3}$ for the parallel case and $|d_\perp/d_{14}| \leq 1$ for the perpendicular case [18–20]. The correlation 2D map of Fig. 1(b) shows that numerous grains
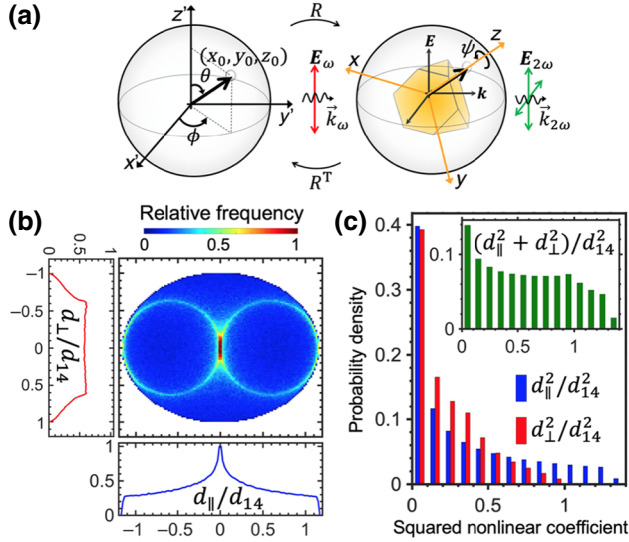
FIG. 1. (a) A schematic of the random rotation from laboratory coordinates (x', y', z') to crystal coordinates (x, y, z) and vice versa. (b) Correlation of the nonlinear coefficient in a randomly oriented single crystal between orthogonal polarizations and their projected 1D histograms. (c) The probability of the normalized squared nonlinear coefficients for parallel and perpendicular polarizations and their sum.

do not contribute to SHG, whereas there is a nonzero probability for the grains to align with the [1 1 1] direction, which maximizes the nonlinearity and produces polarization contributing to the "parallel" SH component. Figure 1(c) shows the distribution of the squared nonlinear coefficient, normalized to d_{14}^2, for parallel and perpendicular polarizations and their combination (if no polarizer at the output is used). Table I shows the expected values of the modulus and the squared value of the nonlinear coefficient. We note that the total (parallel plus perpendicular polarizations added) squared effective nonlinear coefficient is $0.57 d_{14}^2$, which is substantially larger than the value $0.14 d_{14}^2$ given in Ref. [7].

III. EXPERIMENT AND RESULTS

The focus of our experimental study is ZnSe—a zinc-blende structure with a large coherence length, related to our specific application in ultrafast midinfrared OPOs. First, we characterize the nonlinear optical properties of ZnSe ceramics through the SHG process (from 4.7 to 2.35 μm) using a nanosecond OPO source at $\lambda = 4.7$ μm

TABLE I. The expected value of the nonlinear coefficient in a randomly oriented single grain.

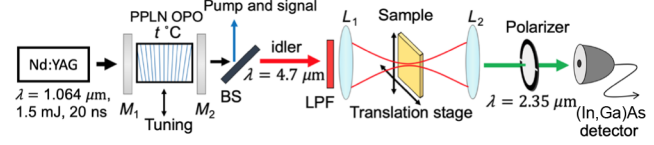| $|d_\parallel / d_{14}|$	$|d_\perp / d_{14}|$	$d_\parallel^2 / d_{14}^2$	$d_\perp^2 / d_{14}^2$	$(d_\parallel^2 + d_\perp^2) / d_{14}^2$
0.48	0.41	0.34	0.23	0.57

FIG. 2. The experimental setup for characterization of polycrystalline ZnSe via SHG. The PPLN OPO is tuned to select the idler wave of 4.7 μm. The beam splitter (BS) and the long-pass filter (LPF) reject the OPO signal and the pump beams and transmit the OPO idler wave. The beam is focused by a $f = 50$ mm CaF$_2$ lens (L_1). A ZnSe sample is placed at the focus and scanned in the x and y directions. The SH signal is collected by a $f = 50$ mm BK7 lens (L_2) and measured using an (In, Ga)As detector.

(Fig. 2). The OPO is pumped by a $\lambda = 1.064$ μm Q-switched Nd:YAG laser with a pulse duration of 20 ns and a pulse energy of 1.5 mJ, operating at a repetition rate of 100 Hz. The OPO linear cavity contains a fanned-out periodically poled lithium niobate (PPLN) crystal for frequency tuning and produces a linearly polarized idler wave with an energy of about 15 μJ at 4.7 μm, which is focused at normal incidence into an RPM sample. The second harmonic output ($\lambda = 2.35$ μm), produced in a ZnSe ceramic sample, is detected using an "extended" (In, Ga)As detector having a long-wave cutoff at 2.6 μm (thus it is "blind" to the fundamental wave). A metal-grid polarizer is placed before the (In, Ga)As detector to separately measure the two output SH polarizations. Our ZnSe samples are based on commercial chemical-vapor-deposition- (CVD) grown ZnSe ceramics, where the optimal average grain size is close to the coherence length (102 μm) of our studied nonlinear processes and is achieved by thermal annealing in vacuum at 900 °C [11]. The samples are cut and polished to a 5×10 mm cross section and their thickness varies between 0.5 and 2 mm. The surface of a chemically etched sample revealing the grain structure is shown in Fig. 3(a).

To measure the grain-size distribution, we analyze microscope image of the etched surface using the linear intercept method. The average grain size is 95 μm, with a standard deviation of 48 μm. The distribution is best fitted with the lognormal function, as shown in Fig. 3(b). The samples are mounted on an XY translation stage at a focal plane, and the SH intensity for the parallel and perpendicular polarizations is 2D mapped using 100-μm steps. The pump beam size is 50 μm [full width at half maximum (FWHM)] and the depth of the focal region is greater than the crystal thickness.

A typical mapping result for a 1-mm-long sample (with the SH polarizations parallel and perpendicular to that of the pump) is shown in Fig. 4(a). One can see numerous "hot spots," where the SH intensity is much higher than the average. These hot spots can be used for applications requiring high nonlinear gain. Figure 4(b) plots the average SH power (parallel SH polarization) for different lengths
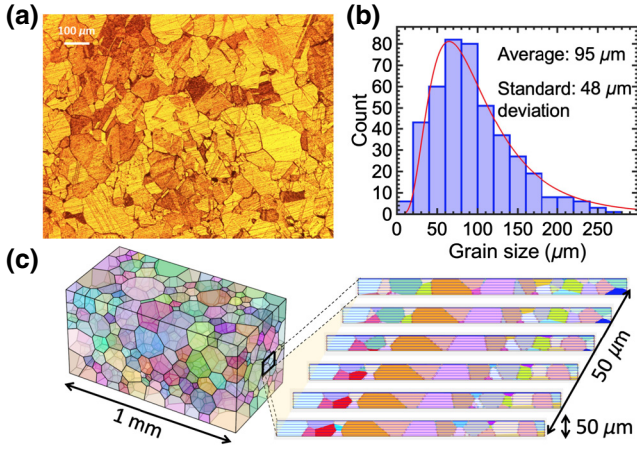
FIG. 3. (a) The cross section of a chemically etched ZnSe ceramic sample (total size 1.2×0.9 mm). (b) The histogram for the grain-size distribution, which is measured using the line intercept method: solid line, lognormal fit. (c) A modeled polycrystalline structure created by Voronoi tessellation, where different colors correspond to different orientations of grains (left) and an example of a sliced $50 \ \mu$m $\times 50 \ \mu$m $\times 1$ mm structure that is used for $w \approx D$ simulation (right).

of samples (which are all from the same origin). The linear dependence on the sample length confirms the prediction of the RPM theory [2]. The ratio of the average SH power for the parallel and perpendicular polarizations $P_{\parallel}^{2\omega}/P_{\perp}^{2\omega}$ varies from 1.2 to 2.1 for different samples. Interestingly, when the samples are rotated by $90°$ in the plane perpendicular to the beam and the two measurements are averaged, the ratio becomes closer to 1.5, which is in accord with the simulated average value, as described below. The fact that the ratio $P_{\parallel}^{2\omega}/P_{\perp}^{2\omega}$ is not the same for different orientations indicates that the grain size and orientation are not purely random. The possible anisotropy can be due to a selected growth direction in the CVD process. The histograms of the SH power for both output polarizations are shown in Fig. 4(c). (The normalizing factor is such that the average power for the parallel polarization is 1.)

IV. SIMULATIONS

RPM is numerically investigated for the two conditions in terms of the beam size w compared to the average grain size D. The model assumes the wave equation under the plane wave and nondepleted approximation, together with the derived random susceptibility tensor and a real grain-size distribution. Additionally, for analyzing the variation of second-harmonic (SH) polarization through the randomly modified tensor, we consider two orthogonally polarized output waves in the plane, transverse to the propagation direction [21]. First, we assume that the beam size is much smaller than the average grain size, which
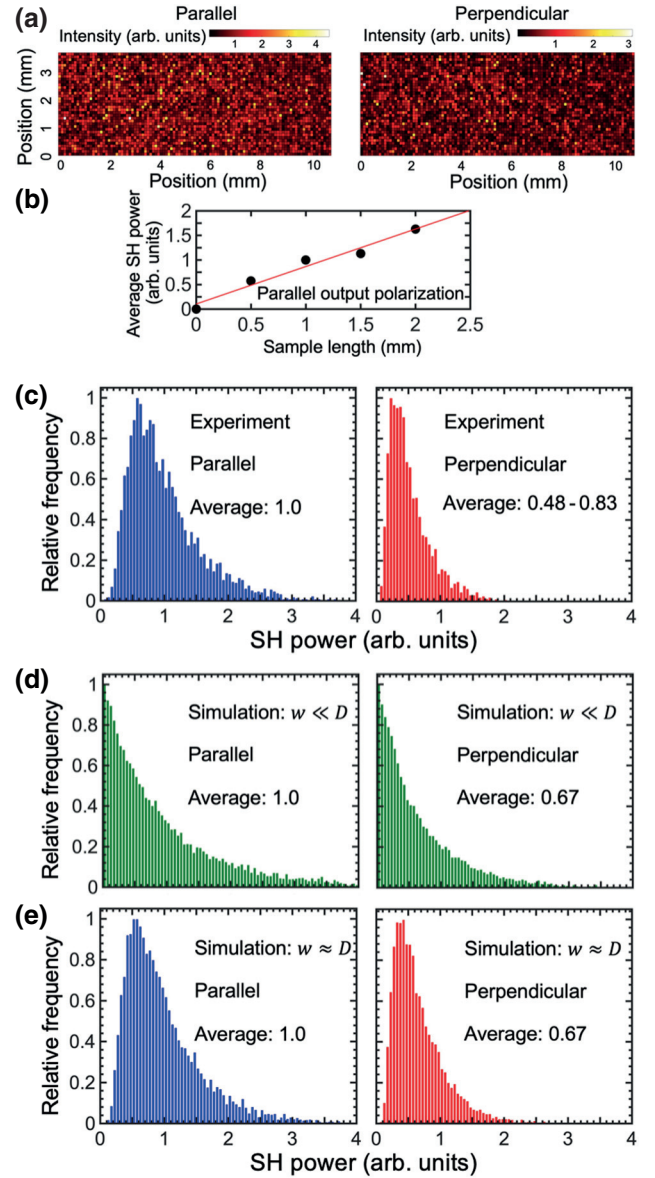

FIG. 4. (a) A 2D color-coded plot for the relative SH power obtained by scanning a 1-mm-long sample with a 100-μm step for both parallel and perpendicular components. (b) The length dependence of the average SH power. (c) The histogram of the SH power obtained from the mapping. The average values are 1.0 for parallel and 0.53 for perpendicular polarization, and their ratio in this case is 1.9. (d),(e) Simulated histograms of the normalized SH power for the parallel and perpendicular components in the cases of $w \ll D$ and $w \approx D$.

is typically the case for high-repetition-rate ultrafast interactions. In this way, we perform 1D simulations along the beam-propagation direction. The simulated histogram of Fig. 4(d) shows a higher probability of weak SH signals as compared to experiment [Fig. 4(c)]. This mismatch derives from the fact that the beam inside the sample has a finite cross section and thus can "see" several grains at a time. To analyze this effect, a polycrystalline structure model is

created by Voronoi tessellation, as shown in Fig. 3(c) [22]. It is based on a real ZnSe sample, in terms of the distribution of the grain size and the orientation. In this simulation, we assume a real beam size (50 μm) and perform multiple 1D simulations using 10-μm steps in the transverse plane, assuming that the nonlinear polarizations induced in the neighboring grains (in the transverse plane) are uncorrelated. An example of a 50 μm × 50 μm × 1 mm structure that is sliced into several cross sections along the beam-propagation direction is shown in Fig. 3(c). The simulated SH power histogram that takes averaging over the beam cross section into account, shown in Fig. 4(e), demonstrates good agreement with the experiment [Fig. 4(c)] in terms of the histogram shape and the ratio $P_{\parallel}^{2\omega}/P_{\perp}^{2\omega}$. For large beams, $w \gg D$, the variation of the output signal is expected to be even smaller due to the averaging effect in the transverse plane.

V. RANDOM-PHASE VS QUASI-PHASE-MATCHING

As predicted earlier [13] and demonstrated experimentally [9–12], RPM is very well suited for ultrafast three-wave interactions. In fact, the group-delay walk-off between the waves with different center wavelengths, especially when few-optical-cycle laser pulses are used, limits the interaction length to less than 1 mm. Using Monte Carlo simulations, we evaluate the performance of RPM ZnSe for $w \ll D$ by comparing it with QPM. We model
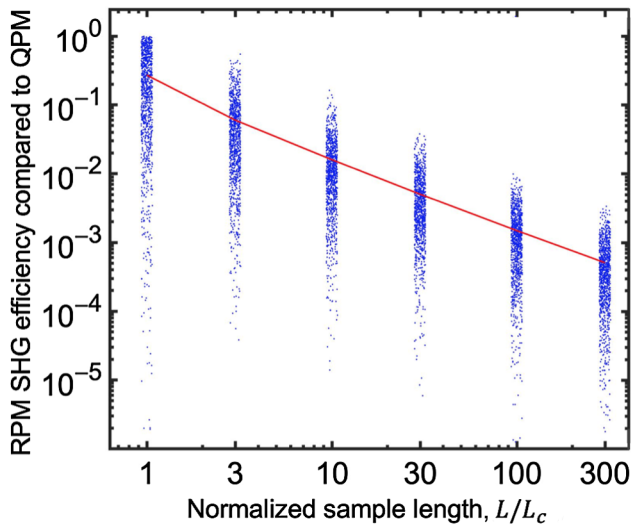

FIG. 5. The RPM SHG efficiency for tightly focused beams normalized to that of an ideal QPM material (only the parallel output component is counted) as a function of the normalized sample length. For each sample length (1, 3, 10, 30, 100, and 300 L_c), the Monte Carlo simulation is performed using 1000 sets of random structures and the average efficiency is shown as a solid line. A nonlinear coefficient of $\sqrt{4/3}d_{14}$ is used for the QPM condition.

an "ideal" ZnSe QPM material that uses a nonlinear coefficient of $\sqrt{4/3}d_{14}$ (the beam propagates along [1 1 0] and all polarizations are along [1 1 1], by analogy with GaAs [19]). Figure 5 shows the RPM SHG efficiency for different sample lengths, normalized to that of an "ideal" QPM crystal of the same length. One can see that the RPM vs QPM efficiency quickly degrades with the sample length (as $1/L$); however, for shorter interaction lengths, there is a greater chance that RPM can perform on a par with QPM. For example, at $L < 5L_c$, the SHG efficiency at the RPM hot spots can reach 50% of that of an ideal QPM crystal. This is totally consistent with the measured pump threshold in the femtosecond OPO that was based on RPM ZnSe and pumped at $\lambda = 2.35$ μm, demonstrated in Ref. [11]. Given the effective length for a nonlinear interaction of approximately 500 μm (5 ZnSe grains), determined by the depth of the focal region of the focused pump beam, and assuming $d_{14} \approx 20$ pm/V for ZnSe, we estimate that the 90-mW OPO pump threshold observed in the experiment is less than 2 times that for an ideal QPM case.

VI. CONCLUSION

We develop a rigorous model for RPM in a zinc-blende structure, which takes into account a realistic distribution of the effective nonlinearity among the grains for both parallel and orthogonal output polarizations, as well as the grain-size distribution. We verify the model's predictions and find a good accord between experiment and theory. We also show that in the case of ultrafast interactions with focused beams, a disordered RPM material can perform on a par with a QPM material. This is especially important for ZnSe, since a QPM ZnSe is not yet available. Overall, RPM in polycrystalline materials opens a route for ultrafast interactions, including frequency up- and down-conversion, as well as producing ultrabroadband midinfrared OPO frequency combs.

ACKNOWLEDGMENTS

[1] J. A. Armstrong, N. Bloembergen, J. Ducuing, and P. S. Pershan, Interactions between light waves in a nonlinear dielectric, Phys. Rev. **127**, 1918 (1962).

[2] S. K. Kurtz and T. T. Perry, A powder technique for the evaluation of nonlinear optical materials, J. Appl. Phys. **39**, 3798 (1968).

[3] C. K. N. Patel, Optical Harmonic Generation in the Infrared Using a CO_2 Laser, Phys. Rev. Lett. **16,** 613 (1966).

[4] R. Hellwarth and P. Christensen, Nonlinear optical microscopic examination of structure in polycrystalline ZnSe, Opt. Commun. **12,** 318 (1974).

[5] R. Kesselring, A. W. Kälin, and F. K. Kneubühl, Mid-infrared nonlinear phenomena in polycrystalline semiconductors, Appl. Phys. B **55,** 437 (1992).

[6] T. D. Chinh, W. Seibt, and K. Siegbahn, Dot patterns from second-harmonic and sum-frequency generation in polycrystalline ZnSe, J. Appl. Phys. **90,** 2612 (2001).

[7] M. Baudrier-Raybaut, R. Haïdar, P. Kupecek, P. Lemasson, and E. Rosencher, Random quasi-phase-matching in bulk polycrystalline isotropic nonlinear materials, Nature **432,** 374 (2004).

[8] R. Kupfer, H. J. Quevedo, H. L. Smith, L. A. Lisi, G. Tiwari, C. G. Richmond, B. B. Bowers, L. Fang, and B. M. Hegelich, Cascade random-quasi-phase-matched harmonic generation in polycrystalline ZnSe, J. Appl. Phys. **124,** 243102 (2018).

[9] S. Vasilyev, I. Moskalev, M. Mirov, S. Mirov, and V. Gapontsev, Three optical cycle mid-IR Kerr-lens mode-locked polycrystalline Cr^{2+}:ZnS laser, Opt. Lett. **40,** 5054 (2015).

[10] S. Vasilyev, I. Moskalev, V. Smolski, J. Peppers, M. Mirov, V. Fedorov, D. Martyshkin, S. Mirov, and V. Gapontsev, Octave-spanning Cr:ZnS femtosecond laser with intrinsic nonlinear interferometry, Optica **6,** 126 (2019).

[11] Q. Ru, N. Lee, X. Chen, K. Zhong, G. Tsoy, M. Mirov, S. Vasilyev, S. B. Mirov, and K. L. Vodopyanov, Optical parametric oscillation in a random polycrystalline medium, Optica **4,** 617 (2017).

[12] R. Šuminas, G. Tamošauskas, G. Valiulis, V. Jukna, A. Couairon, and A. Dubietis, Multi-octave spanning nonlinear interactions induced by femtosecond filamentation in polycrystalline ZnSe, Appl. Phys. Lett. **110,** 241106 (2017).

[13] E. Y. Morozov and A. S. Chirkin, Stochastic quasi-phase matching in nonlinear-optical crystals with an irregular domain structure, Quantum Electron. **34,** 227 (2004).

[14] X. Vidal and J. Martorell, Generation of Light in Media with a Random Distribution of Nonlinear Domains, Phys. Rev. Lett. **97,** 013902 (2006).

[15] R. W. Boyd, *Nonlinear Optics*, 3rd ed., (Academic Press, New York, 2008).

[16] F. Zernike and J. E. Midwinter, *Applied Nonlinear Optics* (Wiley, New York, 1973).

[17] G. Marsaglia, Choosing a point from the surface of a sphere, Ann. Math. Stat. **43,** 645 (1972).

[18] T. Skauli, K. L. Vodopyanov, T. J. Pinguet, A. Schober, O. Levi, L. A. Eyres, M. M. Fejer, J. S. Harris, B. Gerard, L. Becouarn, E. Lallier, and G. Arisholm, Measurement of the nonlinear coefficient of orientation-patterned GaAs and demonstration of highly efficient second-harmonic generation, Opt. Lett. **27,** 628 (2002).

[19] K. L. Vodopyanov, O. Levi, P. S. Kuo, T. J. Pinguet, J. S. Harris, M. M. Fejer, B. Gerard, L. Becouarn, and E. Lallier, Optical parametric oscillation in quasi-phase-matched GaAs, Opt. Lett. **29,** 1912 (2004).

[20] K. L. Vodopyanov, Polarization-insensitive nonlinear-optical devices, Proc. SPIE **6875,** 68750 (2008).

[21] P. S. Kuo and M. M. Fejer, Mixing of polarization states in zincblende nonlinear optical crystals, Opt. Express **26,** 26971 (2018).

[22] R. Quey, P. R. Dawson, and F. Barbe, Large-scale 3D random polycrystals for the finite element method: Generation, meshing and remeshing, Comput. Methods Appl. Mech. Eng. **200,** 1729 (2011).